

Temporal defects and topological transitions in parametric oscillations: theory and experiments

Benjamin Apffel^{1,2} and Romain Fleury¹

¹Institute of Electrical and Micro Engineering, Laboratory of Wave Engineering, Ecole Polytechnique Fédérale de Lausanne (EPFL), Station 11, 1015 Lausanne, Switzerland

²E-mail address: benjamin.apffel@epfl.ch

September 8, 2023

Abstract

Parametric oscillators are examples of non-linear externally driven systems that can exhibit two oscillating limit cycles with opposite phase depending on the initial conditions. In this work, we propose to study what happens to such oscillator initially in one of its limit cycle when the external forcing is perturbed by a defect parametrized by a continuous parameter. The oscillator will be perturbed by the defect and finally reach another limit cycle, which phase can either be the initial one or the opposite one depending on the value of the parameter. For some critical value of the later, a transition therefore occurs and the oscillation amplitude vanishes while a typical time response of the system diverges. Those features are reminiscent of phase transitions in condensed matter, and a topological interpretation in terms of winding number in the phase space is proposed. Complete transition diagrams are computed numerically and measured experimentally using parametric Faraday instability at the surface of a vibrated fluid. The results discussed in the present work can be generalized to any system that admits a finite number of limit cycles.

1 Introduction

The parametric oscillator is one of the simplest non-linear externally driven system, a paradigmatic example being a pendulum shaken vertically at at twice its resonance frequency. Parametric oscillators are encountered in many different fields of physics including quantum mechanics [5, 23, 29], optics [1, 13], (micro-)mechanics [15, 6, 24, 26], electronics [4] or hydrodynamics [9, 8], making their study of prime interest. The rich physics of this system results from complex interactions between damping, forcing and non-linearity. The response amplitude of the system strongly depends on the exact parameters of the system and can exhibit (among others) linear stability around zero, sub-critical or super-critical Hopf bifurcation toward a finite amplitude oscillation, sub-harmonic oscillation, bistability and hysteresis [10, 8]. For a given configuration, the amplitude response when the external forcing is perturbed has also been investigate recently in the context of time crystal [7, 20].

In parallel to the amplitude behavior, the phase response of the system has also been investigate in several regimes. In the linearly stable regime, it can for instance be used to perform squeezing of noise in thermal [24] and quantum [23, 29] regimes. In the sub-harmonic finite amplitude oscillation regime, the oscillation phase is fixed by the forcing and can only take two discrete values separated by π . This phase degeneracy has for instance been used as an analog bit to store information [14, 25], or to simulate the two states of a 1/2-spin in coherent Ising machines to compute the ground state of Hamiltonians [27, 16, 17, 28, 22]. In this context, several strategies to perform bit-flipping (or phase switch) have been implemented by perturbing the excitation signal in a specific manner [21, 12].

The purpose of the present work is to systematically study the condition for a phase switch to occur by considering a continuously parametrized family of perturbations (or time defects). We show that there exist some specific critical values of the defect parameter, close to which the parametric oscillator either perform a phase switch or not, resulting in a transition of the system's behavior. In particular, we aim to describe here how the system switches between its different discrete phase states

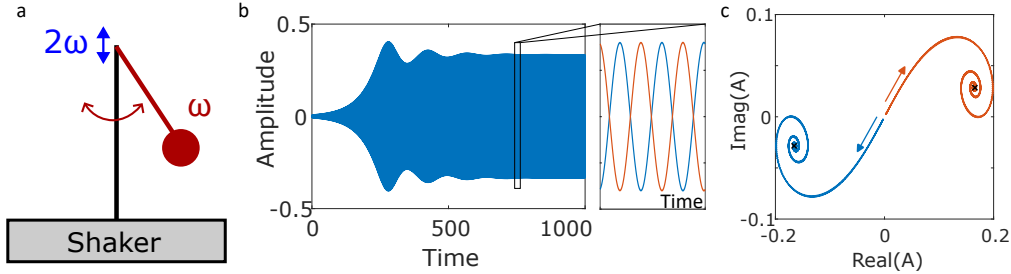


Figure 1: **Parametric oscillation and phase degeneracy.** (a) An example of a parametric oscillator: a pendulum with natural pulsation of ω vibrated at 2ω . (b) Angular position of the pendulum evolving according to Eq. 1 for $\omega = \pi$, $\epsilon = 0.03$ and $\omega\tau = 200$. After an exponential growth, the amplitude oscillates and eventually saturates to a limit value due to non-linearities. Inset: two possible phases can be observed once the system has reached a limit cycle depending on the initial conditions. (c) The limit cycle being harmonic at low forcing, one can associate a complex phasor to the dynamic that reaches one of the two possible complex values $\pm A_c$ at long time.

when the defect parameter is continuously changed near such transition. Interestingly, several features of topological phase transitions usually predicted in condensed matter can be observed in this system along the time dimension.

The paper is organized as follow. We first introduce some useful formalism to study parametric oscillators and define our family of time defects. We then show that there exists some critical values of the parameter that separate no phase switch to phase switch behavior, giving rise to a transition with respect to the defect parameter. Interestingly, we show that this transition exhibits topological properties. We then compute numerically transition diagrams and discuss the role of non-linearity in the observed domains. Last, we present an experimental realization of these concepts using Faraday instability, for which a complete transition diagram is measured experimentally. We finish the article with possible generalization and applications of our findings.

2 Temporal defects and parametric oscillators

2.1 Phase degeneracy of a parametric oscillator

We start here with reminders on parametric oscillators and phase degeneracy, which will be the key ingredient for the rest of the article. Let us consider a parametric oscillator as depicted in figure 1a that consists in a pendulum with natural pulsation ω and vibrated at 2ω . The evolution equation for the angular coordinate ψ is then

$$\frac{d^2\psi}{dt^2} + \frac{2}{\tau} \frac{d\psi}{dt} + \omega^2(1 + \epsilon \cos(2\omega t)) \sin(\psi) = 0 \quad (1)$$

where τ is the damping time and ϵ is the adimensioned forcing amplitude. Let us assume for now that both the forcing and the damping are small $\epsilon, 1/\omega\tau \ll 1$, and that the initial conditions are small, for instance ($\psi \ll 1, \dot{\psi} = 0$). In that case, one can linearize Eq. (1) and show that there exists a critical forcing ϵ_c such that for $\epsilon > \epsilon_c$, the angular position of the pendulum will oscillate at ω while exponentially growing with a slow time scale $\sim 1/\omega\epsilon$ (see SI). This exponential growth will last until the non-linearity becomes non-negligible. The latter will eventually saturate the oscillation amplitude, and the oscillator eventually reaches a limit cycle with finite amplitude as shown in Fig. 1b.

An important feature of this limit cycle is that its oscillation phase is not arbitrary but rather fixed by the phase of the forcing. This is directly related to the time-translation symmetry breaking induced by the forcing. Nevertheless, the evolution equation is still invariant under the discrete symmetry $t \rightarrow t + T$ with T the forcing period. As a consequence, if one has a solution $\psi(t)$ that oscillates with period $2T$ and phase ϕ , another solution $\psi(t+T) = -\psi(t)$ is immediately associated to it through the discrete symmetry. There is therefore not one but two possible phases for the sub-harmonic oscillation that are ϕ or $\phi + \pi$. This 2-fold phase degeneracy is directly related to the 2:1 resonance between the forcing and the pendulum. The choice of one phase or the other is completely determined the initial

conditions. We show in Fig. 1b the existence of those two phases by performing a direct simulation of Eq. 1 with the same forcing but opposite initial conditions for the pendulum's position.

As mentioned before, the saturation of the amplitude is directly related to the non-linearity in Eq. 1. As $\epsilon \ll 1$, one can moreover show that the limit cycle is to first order harmonic in ω , meaning that one can write for long time $\psi(t) = A_c e^{i\omega t} + A_c^* e^{-i\omega t}$ while $\dot{\psi} = i\omega(A_c e^{i\omega t} - A_c^* e^{-i\omega t})$ (see SI for details and comprehensive proofs). As we aim here to focus on the phase chosen by the system rather than on its oscillation, we introduce the complex amplitude $A(t)$ through the invertible transformation

$$\psi(t) = A(t)e^{i\omega t} + A(t)^* e^{-i\omega t} \quad (2)$$

$$\dot{\psi}(t) = i\omega A(t)e^{i\omega t} - i\omega A(t)^* e^{-i\omega t} \quad (3)$$

The amplitude $A(t)$ associated to Fig. 1b is plotted in Fig. 1c. When a harmonic limit cycle is reached, the complex amplitude reaches as expected a constant value $\pm A_c$ depending on the initial conditions. This makes those variables particularly convenient to study the phase of limit cycles, as the two different possible phases of the oscillation are associated to different fixed points in the complex plane. In what follows, we will therefore refer to those two points as the 'phase states' of the system.

2.2 Introducing a temporal defect

Let us assume that the parametric oscillator runs for a long time for $t < 0$ so that it has reached one of its phase state, meaning that $A(0)$ is equal to, say, A_c . We now assume that for $0 < t < T$ we perturb the forcing of the system by adding a temporal defect parametrized by λ , that we will refer to as the defect parameter. Formally, this corresponds to perform the substitution $\epsilon \cos(2\omega t) \rightarrow \epsilon \cos(2\omega t) + g_\lambda(t)$ in Eq. 1, with $g_\lambda(t)$ being non-zero only for $0 < t < T$. For instance, if $g_\lambda(0 < t < T) = \lambda \cos(2\omega t)$, the defect corresponds to increase the forcing amplitude from ϵ to $\epsilon + \lambda$ during a time T . Hereafter, we will rather consider defects on the excitation frequency. For this, we will perturb at $t = 0$ the excitation frequency from 2ω to $2\omega(1 + \lambda)$ during a time $T_\lambda = \pi/\omega\lambda$, the natural frequency of the pendulum remaining the same. Doing so, the perturbed excitation takes an overall phase of 2π during T_λ compared to the unperturbed signal, as shown in Fig. 2a-b. After T_λ , the perturbed excitation is back in phase with the unperturbed one and the excitation frequency is set back to 2ω . This particular choice of T_λ ensures (1) the continuity of the excitation signal as shown in Fig. 2a-b and (2) that the possible phase states of the oscillator are the same before and after the defect, since they are completely determined by the phase of the forcing.

3 Transition with respect to the defect parameter

3.1 Definition and topological aspects of the transition

Adding this defect will perturb the parametric oscillator from its limit cycle and thus $A(t)$ will start to move in the complex plane. After the end of the defect, if one waits long enough the system will reach another phase state, that can either be the one it started from or the other one. Depending on the value of λ , both phase states can be reached as shown in fig. 2 c-d. The evolution of the associated complex amplitude $A(t)$ is shown in Fig. 2e. Starting from one fixed point, the system eventually reaches one of the two possible fixed point $A(\infty) = \pm A_c$. The phase difference between $A(0)$ and $A(\infty)$ must be a multiple of π whatever the defect that has been introduced. This motivates to define a quantized quantity Q as the number of half turns done by the trajectory

$$Q(\lambda) = \frac{1}{\pi} \Im \left(\log \frac{A(\infty)}{A(0)} \right) \quad (4)$$

that must be an integer. Although we focus here on the particular case of parametric oscillator, note that such definition could be extended in a straightforward manner to other systems with a finite number of attractive limit cycles for which a phase can be defined. The system would be forced to converge to one of the cycle before and after the defect, forcing the quantization of the phase difference between the initial and the final state. In the same manner, the particular choice of non-linearity made here is not particularly relevant, the only important feature being once again the existence of finite number limit cycles (two in our case).

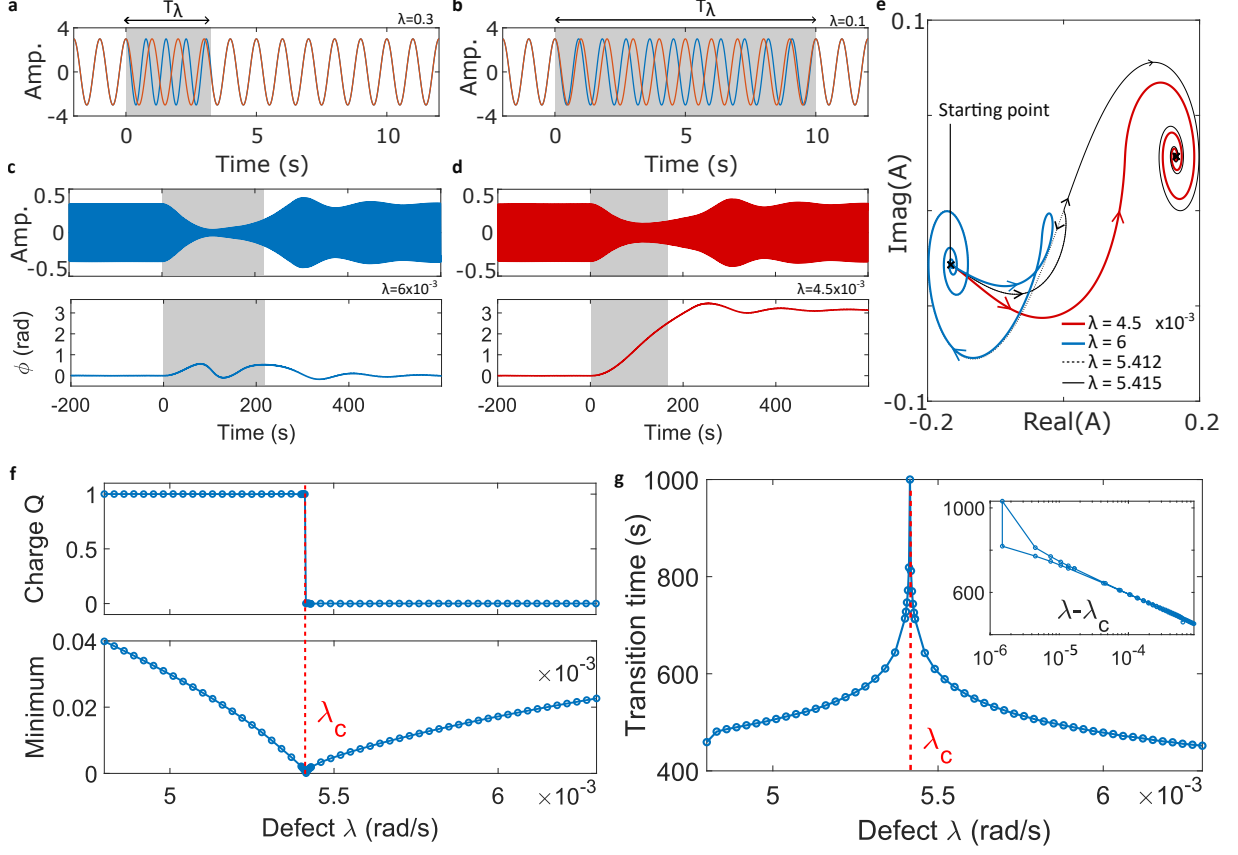


Figure 2: **Temporal defects and topological transition.** (a-b) Two examples of defects for (a) $\lambda = 0.1$ and (b) $\lambda = 0.3$ (blue curves), the unperturbed excitation being plotted for comparison in red. The duration of the detuning is chosen so that the two excitation signals collapse back together after T_λ . (c) Simulated evolution of the parametric oscillator for $\epsilon = 0.03$, $\lambda = 6 \times 10^{-3}$ and (d) $\lambda = 4.5 \times 10^{-3}$, the grey area corresponding to the defect duration. The phase of the corresponding complex amplitude is shown below, and the change of phase state only occurs for the second case. (e) Trajectories in the complex amplitudes for $\epsilon = 0.03$ and different values of $\lambda = [4.5; 5.412; 5.415; 6.0] \times 10^{-3}$. The system is initially in one phase state and reaches after the defect one or the other phase state depending on the value of λ . (f) Phase difference Q between $A(\infty)$ and $A(0)$ (normalized by $1/\pi$) and minimum amplitude of the field for different values of defect λ , the forcing $\epsilon = 0.03$ being fixed. At the critical value λ_c , the field cancels out and Q goes from an integer value to another. (g) Transition time for the system to converge back to its final phase state (see SI for details). The time diverges at the critical value λ_c . Inset: semilog scale plot of the transition time as a function of $\lambda - \lambda_c$ with $\lambda_c = 5.415 \times 10^{-3}$ estimated from (e), showing the exponential scaling of the transition time.

The dependency of Q with respect to the defect parameter λ , the forcing amplitude ϵ being fixed, is shown in Fig. 2f. We see that it is constant on large domains and varies suddenly from one integer value to another for a critical value λ_c . The complex trajectories corresponding to defect parameters slightly smaller or bigger than this critical value are shown in Fig. 2d (black lines). The transition from no phase-switch to phase switch is clearly visible and is associated to an almost zero value of the complex amplitude at some point. This can be shown quantitatively by computing $\min_{t>0} |A(t)|$ for different values of the defect parameter. As shown in Fig. 2e, the minimum reaches zero exactly when Q changes its value, and corresponds to the case where a winding can not be defined. Such behavior is reminiscent of what typically occurs in condensed matter during a topological phase transition. However in the latter case, most of the predictions are made in the linear regime while the topological invariants is typically written as an integral over the reciprocal space [2, 18, 11]. This is in strong contrast with our system that is intrinsically non-linear, with an integral that runs over time and a (half-)winding that occurs in the phase space.

In order to clarify the topological nature of the transition, one can first remark that if one writes $A(t) = a(t)e^{i\phi(t)}$, one has $Q(\lambda) = \frac{1}{\pi} \int_0^\infty d\phi$. It can therefore be seen as the winding index of the trajectory in the complex plane, the starting point being a fixed phase state and the final point one of the two possible phase state. This expression is only valid if A never cancels out in order to define properly its phase at all time. Under this perspective, it is not so surprising that the field needs to cancel out in order for Q to change its value. To make this statement more precise, one can express Q by writing the evolution equation as $\ddot{\psi} = f_\lambda(\psi, \dot{\psi}, t, \lambda)$. Next, we use Eq. 3 to write $\ddot{\psi} = i\omega \dot{A}e^{i\omega t} + h.c. - \omega^2\psi$. On the other hand, one has $\dot{\psi} = \dot{A}e^{i\omega t} + h.c. + \dot{\psi}$ so that $\dot{A}e^{i\omega t} + h.c. = 0$. Combining those equations, one finally gets the evolution equation for the complex amplitude

$$\dot{A} = \frac{1}{2i\omega} \tilde{f}_\lambda(A, A^*, t)e^{-i\omega t} \quad (5)$$

with $\tilde{f}_\lambda(A, A^*, t) = f(Ae^{i\omega t} + A^*e^{-i\omega t}, i\omega Ae^{i\omega t} - i\omega A^*e^{-i\omega t}, t)$.

Let us now assume that $A(t)$ never cancels, which is equivalent by Eq. 3 to assume that $(\psi, \dot{\psi}) \neq (0, 0)$ at all time. In this case, one can divide the evolution equation by A and integrate it between 0 and ∞ to get

$$Q(\lambda) = \int_0^\infty \Im \left(\frac{\tilde{f}_\lambda(A, A^*, t)}{2i\pi\omega A} e^{-i\omega t} \right) dt \quad (6)$$

This shows that whatever the type of defect that is introduced, there exists a quantity that depends on the trajectory which integral over time is quantized. The only ways to break this quantization is that $A(t)$ either cancels at finite time, so that the integral (6) is ill-defined, or either that $A(t)$ never reaches its final phase state at infinite time, what happens exactly when $A(t = \infty) = 0$. In that case, the quantization in Eq. (6) breaks since the phase of $A(\infty)$ in Eq. (4) is ill-defined. Interestingly, only the second behavior has been observed in our simulations. Whether the first case can happen or not, which would correspond to stopping a parametric oscillation at a finite time with a finite duration defect, is currently under investigation.

A phase transition in condensed matter is typically associated with the divergence of some correlation length at the transition. In our case, such length is replaced by the transition time T_c that it takes for the amplitude $A(t)$ to converge toward its new limit after the defect. This time can be computed numerically (see SI for details on the method) and is plotted in Fig. 2f. We see that this time diverges to infinity when the field reaches zero, that also corresponds to the moment where the transition occurs. Moreover, one can show with a perturbative method in the forcing amplitude $\epsilon \ll 1$ that the scaling of the transition time is expected to be $T_c \sim \log |\lambda - \lambda_c|$ (see SI for details). This scaling is confirmed by numerical results as shown in the inset of Fig. 2f.

3.2 Complete transition diagrams and effect of non-linearity

We now aim to sketch a more general picture of how the winding index Q behaves as a function of the defect parameter λ and the forcing parameter ϵ . In order to ensure that $T_\lambda < T$ for all parameters λ , one can not take λ arbitrarily close from zero as T_λ would diverge. We therefore restrict ourselves to $|\lambda| > \lambda_0$ and distinguish positive and negative values. The resulting transition diagram $Q(\epsilon, \lambda)$ is shown in Fig. 3a. For positive values of λ , the diagram only contains two domains separated by a line, which expression can be fitted as $\lambda_c = 0.12\epsilon + 2.4 \times 10^{-3}$. In the contrary for $\lambda < 0$, more complex

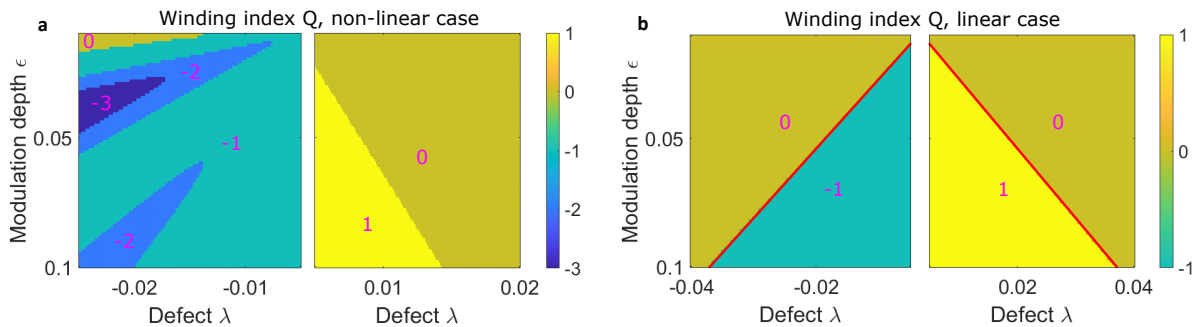


Figure 3: **Numerical computation of transition diagrams.** (a) Transition diagram showing winding index Q in the (ϵ, λ) plane in the non-linear case and (b) in the linear case. The winding index Q only takes integer values that are indicated in the corresponding domains. The red line in the linear case (b) is the analytical prediction computed using perturbative methods.

shapes with larger values of winding index Q appear. We also verified numerically that the transition is always related to a cancellation of the field amplitude at infinite time and to a divergence of the transition time T_c . It is already known that depending on the sign of the detuning, parametric oscillator will experience either subcritical or supercritical bifurcation, breaking the symmetry between positive and negative values of λ [10]. Our results are consistent with such symmetry breaking, although the interplay between the bifurcation type and the transition diagram is not well understood at this stage.

In order to emphasize the role of non-linearity in the shape of the transition diagram, we also compute it when the sinus is linearized in Eq. (1), resulting in a completely linear evolution with respect to ψ . The associated diagram is shown in Fig. 3b. One can see that the phase diagram is completely different as only a single winding transition occurs between $Q = \pm 1$ and $Q = 0$ depending on the sign of the detuning λ . Except for this sign, the phase diagram is moreover symmetric with respect to positive or negative values of λ and the transition curve is a straight line. The evolution equation being linear, one can use perturbative methods to get an analytical prediction for this transition. We show in the SI that the transition occurs for $\lambda_c = \pm 0.34\epsilon$ which is in perfect agreement with direct numerical simulation as shown in Fig. 3b.

The linear case analysis also provides a geometrical interpretation to the winding transition. The technical details are given in SI and we only focus here on the main results. As the evolution is linear, one can write the evolution equation using a 2×2 real matrix evolution and find two eigenvector of the evolution: one being exponentially amplified denoted \vec{e}_+ , the other one being exponentially damped \vec{e}_- . Let us assume that at $t = 0$, the system runs for a long time so that the system is (up to renormalization) in state $A(0) = \vec{e}_+$, where we identify here the complex plane and \mathbb{R}^2 . By adding the defect, one will perturb the eigenvectors of the evolution operator so that at the end of the defect, the system is now in state $A(T_\lambda) = \alpha\vec{e}_+ + \beta\vec{e}_-$. Letting the system evolve again for a long time, the component carried by \vec{e}_- will become negligible so that the system at large time will be (up to positive constant) in state $A(\infty) = \alpha\vec{e}_+$. As the phases of $A(\infty)$ and $A(0)$ are the same up to π , α has to be real but can be either positive or negative, and the sign of α exactly encode the phase difference between the initial and the final state. The key point is then that the vector $A(T_\lambda)$ varies continuously when λ is changed. In particular α goes continuously from positive to negative value when λ goes from zero to infinity (see Fig. 1S in SI). Therefore, the winding transition can be seen as the moment where the projection of $A(T)$ onto \vec{e}_+ exactly cancels out. In this case, A will only have component on \vec{e}_- and exponentially decreases along time, reaching zero for infinite time as observed in our simulations. Of course, this interpretation is only valid in the linear evolution case as one crucially needs to define eigenvectors. It therefore fails to describe what happens in the non-linear regime, in which the transition diagram is strongly modified compared to the linear case.

4 Experimental demonstration

In this last section, we propose an experimental observation of such transition. We take advantage here of the Faraday instability that occurs at the surface of a vibrated fluid [8]. Before coming to the

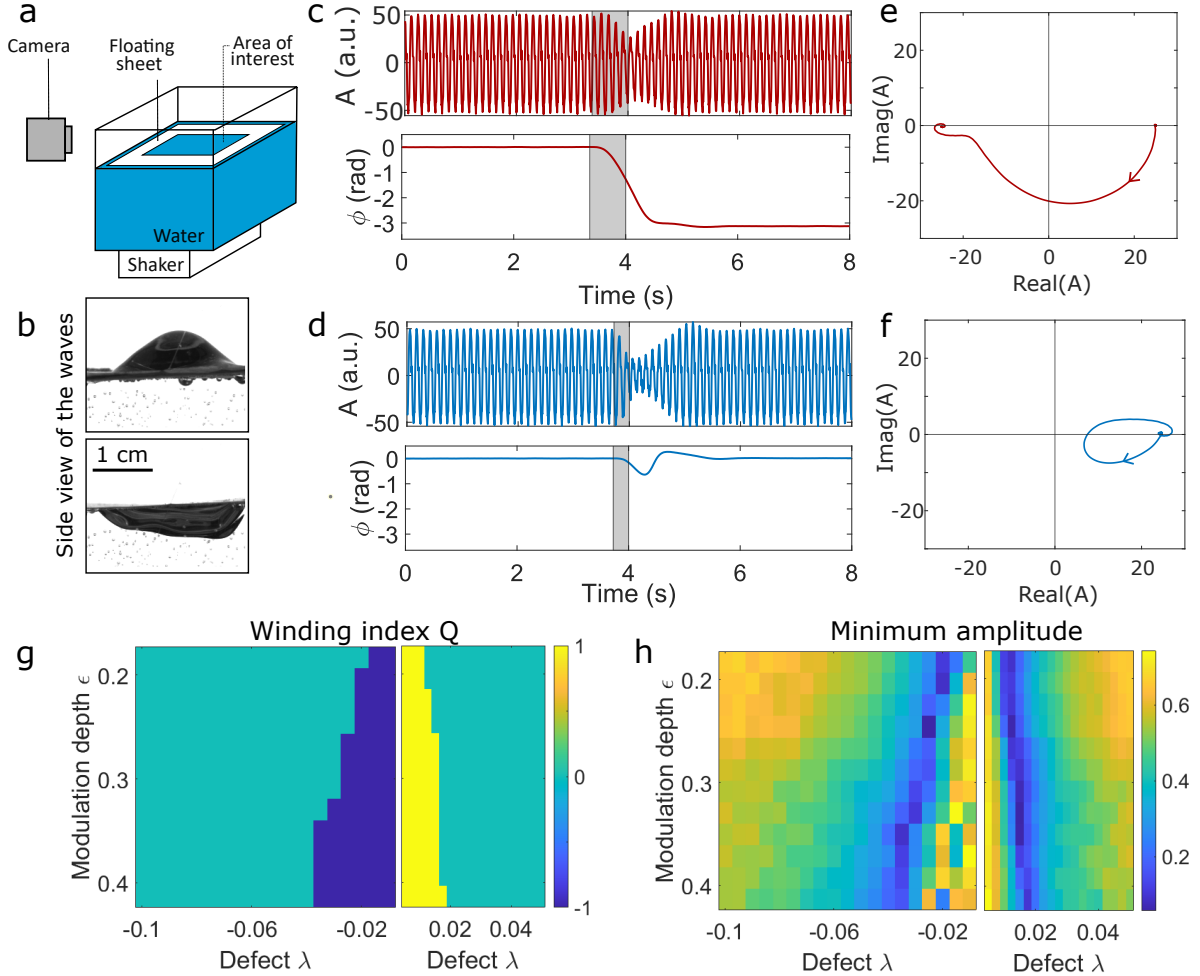


Figure 4: **Experimental demonstration of phase switch and measurement of transition diagrams.** (a) Sketch of the experimental setup: a tank filled with water is placed on a shaker vibrating at 17 Hz. A transparent plastic sheet floating at the surface ensures a good definition of the first parametrically unstable mode at 8.5 Hz. A camera on the side recovers the wave amplitude. (b) Pictures of the parametrically excited waves with opposite phase. (c-d) Experimentally measured wave amplitude along time and the associated complex phase with $\epsilon \approx 0.28$, (c) $\lambda = -0.035$ and (d) $\lambda = -0.015$. The grey area materializes the time defect. A phase switch occurs in (c) but not in (d). (e-f) Associated complex amplitudes showing the winding or not of the trajectory around zero. (g) Experimental transition diagram of Q and (h) associated minimum amplitude of the wave field.

experimental apparatus, we briefly describe here how vibrations can trigger a parametric instability at the surface of a fluid. We assume that the tank is vibrated with an acceleration $a(t) = a \cos(2\omega t)$ and that the perturbations h from the flat surface remain small. In that case, one can linearize the equations of motions and decouple the evolution of each wave vector k , so that the associated Fourier component h_k evolves according to [3] [19]

$$\frac{d^2 h_k}{dt^2} + \frac{2}{\tau} \frac{dh_k}{dt} + \omega_k^2 (1 + \epsilon \cos(2\omega t)) h_k = 0 \quad (7)$$

where τ accounts for viscous dissipation, $\omega_k^2 = gk + \gamma k^3 / \rho$ is given by the gravito-capillary dispersion relation with $g = 9.8 \text{ m/s}^2$ the gravitational acceleration, $\gamma = 60 \text{ mJ/m}^2$ the surface tension and $\rho = 10^3 \text{ kg/m}^3$ the density of water, and the adimensional forcing is given by $\epsilon = \frac{a}{g + \gamma k^2 / \rho}$. This equation is valid as long as the wave field remains small enough. When parametric instability occurs, the wave field will exponentially grow and this hypothesis will eventually break. At this stage, non-linearities will become non-negligible and the wave amplitude will eventually saturate. Although we do not know what type of non-linearity occurs here, the parametric instability provides two distinct limit cycles with a phase difference of π which choice depends on the initial condition. The analysis carried out previously therefore applies and this system can be used to probe the transition with respect to the defect parameter.

The experimental setup consists in a tank of water placed on a shaker driven by a controllable generator at 2ω (see SI for details). Above a given excitation amplitude, the flat surface destabilizes and large amplitude waves oscillating at half the driving frequency appear. In order to avoid frictions on the walls, a transparent plastic sheet pierced with a square hole of $2 \times 2 \text{ cm}$ is placed at the surface as shown in Fig. 4a. The sheet is floating on the water so that evaporation of water does not change the boundary condition of the meniscus, which could impact the experiments [8][7]. The first mode of the square hole occurs at 8.25 Hz and we therefore fix the excitation frequency to 16.25 Hz. Performing experiments show that parametric instability is typically triggered for $a > 2.0 \text{ m/s}^2$ corresponding to a critical adimensioned forcing $\epsilon_c \sim 0.15$. On the other hand, taking a typically greater than 6 m/s^2 leads to unwanted phenomena such as water droplet ejection, giving an upper bound for the reachable forcing $\epsilon \sim 0.5$.

The displacement of the shaker as well as the wave field are recorded using a camera placed on the side. Typical snapshots from a movie are shown in Fig. 4b. From the movies, the wave amplitude can be extracted by analyzing the the image contrast (see SI). The time defect is implemented using the frequency-shift keying (FSK) of the generator, that permits to detune the frequency of the excitation signal to $2\omega(1 + \lambda)$ for the desired time $T_\lambda = \pi / \omega\lambda$. Some typical wave amplitude measurement extracted from the movies are shown in the upper panels on Fig. 4 c-d with $\lambda = -3.5\%$ and $\lambda = -1.5\%$ respectively, the forcing being $\epsilon = 0.30$ in both cases. From these curves, one can compute the associated complex amplitude $A(t)e^{i\phi(t)}$. Its phase $\phi(t)$ is shown in the lower panels of Fig. 4c-d, while the complex amplitude is displayed in Fig. 4e-f. Depending on the value of λ , the trajectory either performs half or no winding around the origin of the complex plane. Together with Fig. 4c-d, the trajectories in the complex plane directly shows whether the waves experienced or not of a phase switch.

Similar measurements can be performed for various values of ϵ and λ in order to obtain the complete transition diagram. The latter is shown in Fig. 4g and clearly exhibits distinct domains with different values of the winding index Q . As in our simulations, there exists a strong asymmetry between positive and negative values of λ , emphasizing the role of non-linearities. However, we did not observe experimentally winding index Q larger than ± 1 . One can nevertheless measure the minimum amplitude of the wave field along time, and our measurements in Fig. 4h confirm that the transition from one winding index to the other is associated with a field cancellation. Our experimental data are moreover in qualitative agreement with an increasing transition time T_c as λ gets closer from its critical value. However, a quantitative agreement with the expected scaling law could not be observed. When the wave amplitude gets close from zero, the presence of non-parametric waves at the water surface may perturb the dynamics of the system. Other experimental systems with less sources of noise are therefore needed to perform such measurement and are currently under investigation.

5 Conclusion and perspective

In this article, we have studied how an active non-linear system that exhibits a discrete number of limit cycles can switch (or not) from one to another by introducing continuously parametrized defects in the excitation. We have shown through the example of the parametric oscillator that the temporal dynamics of the transition exhibits some similarities with phase transitions usually observed in many-body systems. We also gave a topological interpretation of the transition as a change of a winding index in the phase space, and observed it experimentally using fluid mechanics instability.

We see several avenues for the future of this work. First, it would be interesting to consider what happens when the phase space has dimension larger than two, so that the winding index has to be replaced by other topological invariants. We would also like to point out that near the transition, the system is very sensitive to any small change in the value of the defect parameter λ . Such transition may therefore practically be used to perform sensing, providing it is robust enough to noise. On the other hand, understanding the interaction between noise and possible bifurcation between one phase state or the other near the transition is also a promising related topic.

6 Acknowledgment

The authors acknowledge Dr Hervé Lissek for the loan of the shaker and the Grant SNSF Eccellenza 181232 for financial support.

References

- [1] S. Akhmanov et al. “Observation of Parametric Amplification in the Optical Range”. In: *Jetp Letters - JETP LETT-ENGL TR 2* (Jan. 1965).
- [2] Navketan Batra and Goutam Sheet. “Physics with Coffee and Doughnuts”. en. In: *Resonance* 25.6 (June 2020), pp. 765–786. ISSN: 0973-712X. DOI: [10.1007/s12045-020-0995-x](https://doi.org/10.1007/s12045-020-0995-x). URL: <https://doi.org/10.1007/s12045-020-0995-x> (visited on 08/31/2023).
- [3] Thomas Brooke Benjamin, Fritz Joseph Ursell, and Geoffrey Ingram Taylor. “The stability of the plane free surface of a liquid in vertical periodic motion”. In: *Proceedings of the Royal Society of London. Series A. Mathematical and Physical Sciences* 225.1163 (Jan. 1997), pp. 505–515. DOI: [10.1098/rspa.1954.0218](https://royalsocietypublishing.org/doi/10.1098/rspa.1954.0218). URL: <https://royalsocietypublishing.org/doi/10.1098/rspa.1954.0218> (visited on 08/08/2023).
- [4] R. Berthet, A. Petrosyan, and B. Roman. “An analog experiment of the parametric instability”. en. In: *American Journal of Physics* 70.7 (July 2002), pp. 744–749. ISSN: 0002-9505, 1943-2909. DOI: [10.1119/1.1477428](https://pubs.aip.org/ajp/article/70/7/744/1055852/An-analog-experiment-of-the-parametric-instability). URL: <https://pubs.aip.org/ajp/article/70/7/744/1055852/An-analog-experiment-of-the-parametric-instability> (visited on 08/31/2023).
- [5] David C. Burnham and Donald L. Weinberg. “Observation of Simultaneity in Parametric Production of Optical Photon Pairs”. In: *Physical Review Letters* 25.2 (July 1970). Publisher: American Physical Society, pp. 84–87. DOI: [10.1103/PhysRevLett.25.84](https://link.aps.org/doi/10.1103/PhysRevLett.25.84). URL: <https://link.aps.org/doi/10.1103/PhysRevLett.25.84> (visited on 08/31/2023).
- [6] Dustin W. Carr et al. “Parametric amplification in a torsional microresonator”. en. In: *Applied Physics Letters* 77.10 (Sept. 2000), pp. 1545–1547. ISSN: 0003-6951, 1077-3118. DOI: [10.1063/1.1308270](https://pubs.aip.org/apl/article/77/10/1545/515762/Parametric-amplification-in-a-torsional). URL: <https://pubs.aip.org/apl/article/77/10/1545/515762/Parametric-amplification-in-a-torsional> (visited on 08/31/2023).
- [7] Guillaume d’Hardemare, Antonin Eddi, and Emmanuel Fort. “Probing Floquet modes in a time periodic system with time defects using Faraday instability”. en. In: *Europhysics Letters* 131.2 (Aug. 2020), p. 24007. ISSN: 0295-5075. DOI: [10.1209/0295-5075/131/24007](https://dx.doi.org/10.1209/0295-5075/131/24007). URL: <https://dx.doi.org/10.1209/0295-5075/131/24007> (visited on 08/08/2023).
- [8] S. Douady. “Experimental study of the Faraday instability”. en. In: *Journal of Fluid Mechanics* 221 (Dec. 1990), pp. 383–409. ISSN: 1469-7645, 0022-1120. DOI: [10.1017/S0022112090003603](https://www.cambridge.org/core/journals/journal-of-fluid-mechanics/article/abs/experimental-study-of-the-faraday-instability/DB294255CBCDF217BFA024192067E861). URL: <https://www.cambridge.org/core/journals/journal-of-fluid-mechanics/article/abs/experimental-study-of-the-faraday-instability/DB294255CBCDF217BFA024192067E861> (visited on 08/08/2023).

- [9] Michael Faraday. “XVII. On a peculiar class of acoustical figures; and on certain forms assumed by groups of particles upon vibrating elastic surfaces”. In: *Philosophical Transactions of the Royal Society of London* 121 (Jan. 1997). Publisher: Royal Society, pp. 299–340. DOI: [10.1098/rstl.1831.0018](https://royalsocietypublishing.org/doi/10.1098/rstl.1831.0018). URL: <https://royalsocietypublishing.org/doi/10.1098/rstl.1831.0018> (visited on 08/31/2023).
- [10] S. Fauve. “Pattern forming instabilities”. In: *Hydrodynamics and Nonlinear Instabilities*. Ed. by Claude Godrèche and Paul Manneville. Collection Alea-Saclay: Monographs and Texts in Statistical Physics. Cambridge: Cambridge University Press, 1998, pp. 387–492. ISBN: 978-0-521-01763-3. DOI: [10.1017/CB09780511524608.006](https://www.cambridge.org/core/books/hydrodynamics-and-nonlinear-instabilities/pattern-forming-instabilities/3D7AA2DFD014BCD5C172A6FF0278CC00). URL: <https://www.cambridge.org/core/books/hydrodynamics-and-nonlinear-instabilities/pattern-forming-instabilities/3D7AA2DFD014BCD5C172A6FF0278CC00> (visited on 08/18/2023).
- [11] Romain Fleury, Alexander B. Khanikaev, and Andrea Alù. “Floquet topological insulators for sound”. en. In: *Nature Communications* 7.1 (June 2016). Number: 1 Publisher: Nature Publishing Group, p. 11744. ISSN: 2041-1723. DOI: [10.1038/ncomms11744](https://www.nature.com/articles/ncomms11744). URL: <https://www.nature.com/articles/ncomms11744> (visited on 11/14/2022).
- [12] Martin Frimmer et al. “Rapid Flipping of Parametric Phase States”. en. In: *Physical Review Letters* 123.25 (Dec. 2019), p. 254102. ISSN: 0031-9007, 1079-7114. DOI: [10.1103/PhysRevLett.123.254102](https://link.aps.org/doi/10.1103/PhysRevLett.123.254102). URL: <https://link.aps.org/doi/10.1103/PhysRevLett.123.254102> (visited on 01/23/2023).
- [13] J. A. Giordmaine and Robert C. Miller. “Tunable Coherent Parametric Oscillation in LiNbO₃ at Optical Frequencies”. In: *Physical Review Letters* 14.24 (June 1965). Publisher: American Physical Society, pp. 973–976. DOI: [10.1103/PhysRevLett.14.973](https://link.aps.org/doi/10.1103/PhysRevLett.14.973). URL: <https://link.aps.org/doi/10.1103/PhysRevLett.14.973> (visited on 08/31/2023).
- [14] Eiichi Goto. “The Parametron, a Digital Computing Element Which Utilizes Parametric Oscillation”. In: *Proceedings of the IRE* 47.8 (Aug. 1959), pp. 1304–1316. ISSN: 2162-6634. DOI: [10.1109/JRPROC.1959.287195](https://doi.org/10.1109/JRPROC.1959.287195).
- [15] Alvaro A. Grandi, Suzie Protière, and Arnaud Lazarus. “Enhancing and controlling parametric instabilities in mechanical systems”. In: *Extreme Mechanics Letters* 43 (Feb. 2021), p. 101195. ISSN: 2352-4316. DOI: [10.1016/j.eml.2021.101195](https://www.sciencedirect.com/science/article/pii/S2352431621000195). URL: <https://www.sciencedirect.com/science/article/pii/S2352431621000195> (visited on 08/31/2023).
- [16] Toshimori Honjo et al. “100,000-spin coherent Ising machine”. In: *Science Advances* 7.40 (Sept. 2021). Publisher: American Association for the Advancement of Science, eabh0952. DOI: [10.1126/sciadv.abh0952](https://www.science.org/doi/10.1126/sciadv.abh0952). URL: <https://www.science.org/doi/10.1126/sciadv.abh0952> (visited on 11/02/2022).
- [17] Takahiro Inagaki et al. “Large-scale Ising spin network based on degenerate optical parametric oscillators”. en. In: *Nature Photonics* 10.6 (June 2016). Number: 6 Publisher: Nature Publishing Group, pp. 415–419. ISSN: 1749-4893. DOI: [10.1038/nphoton.2016.68](https://www.nature.com/articles/nphoton.2016.68). URL: <https://www.nature.com/articles/nphoton.2016.68> (visited on 08/31/2023).
- [18] Takuya Kitagawa et al. “Topological characterization of periodically driven quantum systems”. In: *Physical Review B* 82.23 (Dec. 2010). Publisher: American Physical Society, p. 235114. DOI: [10.1103/PhysRevB.82.235114](https://link.aps.org/doi/10.1103/PhysRevB.82.235114). URL: <https://link.aps.org/doi/10.1103/PhysRevB.82.235114> (visited on 08/17/2023).
- [19] Krishna Kumar and Laurette S. Tuckerman. “Parametric instability of the interface between two fluids”. en. In: *Journal of Fluid Mechanics* 279 (Nov. 1994), pp. 49–68. ISSN: 1469-7645, 0022-1120. DOI: [10.1017/S0022112094003812](https://www.cambridge.org/core/journals/journal-of-fluid-mechanics/article/abs/parametric-instability-of-the-interface-between-two-fluids/EDFEA4D5AC9660910AC1E99AAC1910FA). URL: <https://www.cambridge.org/core/journals/journal-of-fluid-mechanics/article/abs/parametric-instability-of-the-interface-between-two-fluids/EDFEA4D5AC9660910AC1E99AAC1910FA> (visited on 08/08/2023).
- [20] Eran Lustig, Yonatan Sharabi, and Mordechai Segev. “Topological aspects of photonic time crystals”. EN. In: *Optica* 5.11 (Nov. 2018). Publisher: Optica Publishing Group, pp. 1390–1395. ISSN: 2334-2536. DOI: [10.1364/OPTICA.5.001390](https://opg.optica.org/optica/abstract.cfm?uri=optica-5-11-1390). URL: <https://opg.optica.org/optica/abstract.cfm?uri=optica-5-11-1390> (visited on 10/31/2022).

- [21] I. Mahboob and H. Yamaguchi. “Bit storage and bit flip operations in an electromechanical oscillator”. en. In: *Nature Nanotechnology* 3.5 (May 2008), pp. 275–279. ISSN: 1748-3395. DOI: [10.1038/nnano.2008.84](https://doi.org/10.1038/nnano.2008.84). URL: <https://www.nature.com/articles/nnano.2008.84> (visited on 08/07/2023).
- [22] Peter L. McMahon et al. “A fully programmable 100-spin coherent Ising machine with all-to-all connections”. en. In: *Science* 354.6312 (Nov. 2016), pp. 614–617. ISSN: 0036-8075, 1095-9203. DOI: [10.1126/science.aah5178](https://doi.org/10.1126/science.aah5178). URL: <https://www.science.org/doi/10.1126/science.aah5178> (visited on 09/06/2023).
- [23] G. Milburn and D. F. Walls. “Production of squeezed states in a degenerate parametric amplifier”. In: *Optics Communications* 39.6 (Nov. 1981), pp. 401–404. ISSN: 0030-4018. DOI: [10.1016/0030-4018\(81\)90232-7](https://doi.org/10.1016/0030-4018(81)90232-7). URL: <https://www.sciencedirect.com/science/article/pii/0030401881902327> (visited on 08/31/2023).
- [24] D. Rugar and P. Grütter. “Mechanical parametric amplification and thermomechanical noise squeezing”. en. In: *Physical Review Letters* 67.6 (Aug. 1991), pp. 699–702. ISSN: 0031-9007. DOI: [10.1103/PhysRevLett.67.699](https://doi.org/10.1103/PhysRevLett.67.699). URL: <https://link.aps.org/doi/10.1103/PhysRevLett.67.699> (visited on 08/31/2023).
- [25] Fred Sterzer. “Microwave Parametric Subharmonic Oscillators for Digital Computing”. In: *Proceedings of the IRE* 47.8 (Aug. 1959). Conference Name: Proceedings of the IRE, pp. 1317–1324. ISSN: 2162-6634. DOI: [10.1109/JRPROC.1959.287196](https://doi.org/10.1109/JRPROC.1959.287196).
- [26] Kimberly L. Turner et al. “Five parametric resonances in a microelectromechanical system”. en. In: *Nature* 396.6707 (Nov. 1998), pp. 149–152. ISSN: 1476-4687. DOI: [10.1038/24122](https://doi.org/10.1038/24122). URL: <https://www.nature.com/articles/24122> (visited on 08/07/2023).
- [27] Shoko Utsunomiya, Kenta Takata, and Yoshihisa Yamamoto. “Mapping of Ising models onto injection-locked laser systems”. EN. In: *Optics Express* 19.19 (Sept. 2011). Publisher: Optica Publishing Group, pp. 18091–18108. ISSN: 1094-4087. DOI: [10.1364/OE.19.018091](https://doi.org/10.1364/OE.19.018091). URL: <https://opg.optica.org/oe/abstract.cfm?uri=oe-19-19-18091> (visited on 11/02/2022).
- [28] Zhe Wang et al. “Coherent Ising machine based on degenerate optical parametric oscillators”. In: *Physical Review A* 88.6 (Dec. 2013), p. 063853. DOI: [10.1103/PhysRevA.88.063853](https://doi.org/10.1103/PhysRevA.88.063853). URL: <https://link.aps.org/doi/10.1103/PhysRevA.88.063853> (visited on 08/07/2023).
- [29] Ling-An Wu, Min Xiao, and H. J. Kimble. “Squeezed states of light from an optical parametric oscillator”. EN. In: *JOSA B* 4.10 (Oct. 1987). Publisher: Optica Publishing Group, pp. 1465–1475. ISSN: 1520-8540. DOI: [10.1364/JOSAB.4.001465](https://doi.org/10.1364/JOSAB.4.001465). URL: <https://opg.optica.org/josab/abstract.cfm?uri=josab-4-10-1465> (visited on 08/31/2023).

Supplementary materials: topological transition of phase in parametric oscillators: theory and experiments

Benjamin Apffel¹ and Romain Fleury¹

¹Institute of Electrical and Micro Engineering, Laboratory of Wave Engineering, Ecole Polytechnique Fédérale de Lausanne (EPFL), Station 11, 1015 Lausanne, Switzerland

September 8, 2023

1 Perturbative treatment of a parametric oscillator

1.1 Normal form of the evolution equation

We consider a parametric pendulum with natural frequency ω_0 , damping time τ driven with adimensional acceleration ϵ oscillating at ω and a cubic non-linearity.

$$\frac{d^2\psi}{dt^2} + \frac{2}{\tau} \frac{d\psi}{dt} + \omega_0^2(1 + \epsilon \cos(2\omega t))(\psi - \alpha\psi^3) = 0 \quad (1)$$

For the case of a hanging pendulum, one has $\alpha = 1/6$ to recover the Taylor expansion of $\sin(\psi)$. In all that follows, we will assume that the forcing is small $\epsilon \ll 1$ and expand the solutions with respect to this parameter. We aim to show here that this equation admits two harmonic limit cycles with a difference phase of π when the forcing is small.

We will also assume that the viscous term scales as $2/\tau = \gamma\omega_0\epsilon$ and rescale $\psi = \sqrt{\epsilon}\psi$. The equation can now be written as

$$\frac{d^2\psi}{dt^2} + \gamma\omega_0\epsilon \frac{d\psi}{dt} + \omega_0^2(1 + \epsilon \cos(2\omega t))(\psi - \epsilon\alpha\psi^3) = 0 \quad (2)$$

Last, we set a new time $t \rightarrow \omega_0 t$ so that the equation finally reads

$$\frac{d^2\psi}{dt^2} + \gamma\epsilon \frac{d\psi}{dt} + (1 + \epsilon \cos(2\Omega t))(\psi - \epsilon\alpha\psi^3) = 0 \quad (3)$$

with $\Omega = \omega/\omega_0$. We will now establish an envelope equation using averaging method. For this, we set two complex variables $A(t), A^*(t)$ that we define as

$$\psi(t) = A(t)e^{i\Omega t} + A^*(t)e^{-i\Omega t} \quad (4)$$

$$\partial_t \psi(t) = i\Omega A(t)e^{i\Omega t} - i\Omega A^*(t)e^{-i\Omega t} \quad (5)$$

This transformation is invertible so that there is no hypothesis made at this stage. We are now looking for equations on A and A^* . The first one is given by $\partial_t \psi = \dot{\psi}$ so that

$$\dot{A}e^{i\Omega t} + \dot{A}^*e^{-i\Omega t} = 0 \quad (6)$$

For the second equation, we will recast the equation of motion at first order in ϵ as

$$\frac{d^2\psi}{dt^2} + \Omega^2\psi = -\gamma\epsilon \frac{d\psi}{dt} - \sigma\epsilon\psi - \epsilon \cos(2\Omega t)\psi + \epsilon\alpha\psi^3 = -\epsilon f(\psi, \dot{\psi}, t) \quad (7)$$

with $\sigma = (1 - \Omega^2)/\epsilon \sim 1$. We can then find a second equation on A and A^* as

$$\partial_{tt}\psi = i\Omega\dot{A}e^{i\Omega t} - i\Omega\dot{A}^*e^{-i\Omega t} - \Omega^2\psi \quad (8)$$

so that one finally has

$$i\Omega\dot{A}e^{i\Omega t} - i\Omega\dot{A}^*e^{-i\Omega t} = -\epsilon f(\psi, \dot{\psi}, t) \quad (9)$$

The two equations can be summarized in the matrix form

$$\begin{bmatrix} e^{i\Omega t} & e^{-i\Omega t} \\ i\Omega e^{i\Omega t} & -i\Omega e^{-i\Omega t} \end{bmatrix} \begin{bmatrix} \dot{A} \\ \dot{A}^* \end{bmatrix} = \begin{bmatrix} 0 \\ -\epsilon f \end{bmatrix} \quad (10)$$

and after inverting the matrix, one gets

$$\dot{A} = \frac{i\epsilon}{2\Omega} f(\psi, \dot{\psi}, t) e^{-i\Omega t} \quad (11)$$

1.2 Averaging equation

In equation (11), one has $\dot{A} \sim \epsilon$ so that A varies slowly along time. In that case, one can average the right term of the previous equation over one fast oscillation at Ω_0 . After some computation, one finds

$$\dot{A} = \epsilon \left(-\frac{\gamma}{2} + i\frac{\sigma}{2\Omega} - i\frac{3\alpha}{2\Omega}|A|^2 \right) A + \frac{i\epsilon}{4\Omega} A^* \quad (12)$$

If one assumes now that the unperturbed excitation is perfectly resonant, meaning $\omega = \omega_0$, one has $\Omega_0 = 1$ and $\sigma = 0$. In that case, one has

$$\dot{A} = \epsilon \left(-\frac{\gamma}{2} - i\frac{3\alpha}{2}|A|^2 \right) A + \frac{i\epsilon}{4} A^* \quad (13)$$

If $A \ll 1$, the non-linear term can be neglected and the evolution equation can be expressed as

$$\ddot{A} + \epsilon\gamma\dot{A} + \epsilon^2 \left[\left(\frac{\gamma}{2}\right)^2 - \left(\frac{1}{4}\right)^2 \right] A = 0 \quad (14)$$

This admits solutions of the form

$$A(t) = A_0 e^{(1-2\gamma)\epsilon t/4} + B_0 e^{-(1+2\gamma)\epsilon t/4} \quad (15)$$

Thus we see that the solution exponentially grows if $\gamma < 1/2$ which corresponds to a minimal forcing of

$$\epsilon > \epsilon_c = \frac{4}{\omega_0\tau} \quad (16)$$

As the amplitude will grow, one will not be able to neglect the non-linearity. Due to the latter, the system will reach a limit cycle such that $\dot{A} = 0$. The amplitude reached is fixed by the equation

$$\left(\frac{\gamma}{2} + i\frac{3\alpha}{2}|A|^2 \right) A = \frac{iA^*}{4} \quad (17)$$

that admits a complex solution $A_c \neq 0$ if $\epsilon > \epsilon_c$. Note that $-A_c$ is also solution, showing the degeneracy of the solution. The main point here is that A goes toward one of the two fixed point $\pm A_c$. In particular, the phase of A_c is fixed up to π .

1.3 Adding a time defect

We will now add a time defect in the excitation. For this, we define the detuning function $\phi_d(t) = 2\omega\lambda(t)t$ with $\lambda(t) = \lambda$ for $0 < t < T_\lambda = \pi/\omega\lambda$ and $\lambda(t) = 0$ otherwise. The evolution equation now reads

$$\frac{d^2\psi}{dt^2} + \frac{2}{\tau} \frac{d\psi}{dt} + \omega_0^2 (1 + \epsilon \cos(2\omega t + \phi_d(t))) (\psi - \alpha\psi^3) = 0 \quad (18)$$

Performing the same change of variable as before, we arrive at the evolution equation of the same form as Eq. 11 but that now contains the time defect.

We will now assume once again that the excitation and the pendulum are tuned so that $\Omega = 1$, and that $\phi(t)$ varies slowly compared to the natural oscillation of the pendulum. More precisely, we

will assume that the detuning scales as $\lambda = \beta\epsilon \ll 1$ with $\beta \sim 1$. From this, one can get the averaged adimensionned equation as

$$\dot{A} = \epsilon \left(-\frac{\gamma}{2} - i\frac{3\alpha}{2}|A|^2 \right) A + \frac{i\epsilon}{4} A^* e^{2i\lambda(t)t} \quad (19)$$

We now aim to find the value for λ for which the transition occurs. For this, we will place ourselves in the linear case, meaning $\alpha = 0$. By defining a new amplitude $A(t) \rightarrow A(t)e^{-\epsilon\gamma t/2}$ the evolution equation now becomes

$$\dot{A} = \frac{i\epsilon}{4} A^* e^{2i\lambda(t)t} \quad (20)$$

where $\lambda(t) = \lambda$ for $0 < t < T_\lambda$ (with adimensionned $T_\lambda = \pi/\lambda$) and is zero otherwise. We will now look how the amplitude is modified due to the perturbation. We start with solutions on each time domain

$$A(t) = A_0 e^{\Delta_0 t} + B_0 e^{-\Delta_0/4}, \quad t < 0 \quad (21)$$

$$= A_1 e^{(\Delta_\lambda + i\lambda)t} + B_1 e^{(-\Delta_\lambda + i\lambda)t}, \quad 0 < t < T_\lambda \quad (22)$$

$$= A_2 e^{\Delta_0 t} + B_2 e^{-\Delta_0 t}, \quad T_\lambda < t \quad (23)$$

$$(24)$$

where $\Delta_0 = \epsilon/4$ and $\Delta_\lambda = \sqrt{(\epsilon/4)^2 - \lambda^2}$ (that can be complex). The next thing we need is the continuity equations to go from one solution to the other.

Assuming that A is continuous, \dot{A} will also be continuous according to Eq. 20 and the continuity of $e^{i\lambda(t)t}$ at $t = 0$ and $t = T_\lambda$. From this, one can write the continuity equations at those time

$$\begin{bmatrix} 1 & 1 \\ \Delta_\lambda + i\lambda & -\Delta_\lambda + i\lambda \end{bmatrix} \begin{bmatrix} A_1 \\ B_1 \end{bmatrix} = \begin{bmatrix} 1 & 1 \\ \Delta_0 & -\Delta_0 \end{bmatrix} \begin{bmatrix} A_0 \\ B_0 \end{bmatrix} \quad (25)$$

$$\begin{bmatrix} e^{(\Delta_\lambda + i\lambda)T_\lambda} & e^{(-\Delta_\lambda + i\lambda)T_\lambda} \\ (\Delta_\lambda + i\lambda)e^{(\Delta_\lambda + i\lambda)T_\lambda} & (-\Delta_\lambda + i\lambda)e^{(-\Delta_\lambda + i\lambda)T_\lambda} \end{bmatrix} \begin{bmatrix} A_1 \\ B_1 \end{bmatrix} = \begin{bmatrix} e^{\Delta_0 T_\lambda} & e^{-\Delta_0 T_\lambda} \\ \Delta_0 e^{\Delta_0 T_\lambda} & -\Delta_0 e^{-\Delta_0 T_\lambda} \end{bmatrix} \begin{bmatrix} A_2 \\ B_2 \end{bmatrix} \quad (26)$$

After some computation (and using that $e^{i\lambda T_\lambda} = -1$), one finds

$$\begin{bmatrix} A_2 \\ B_2 \end{bmatrix} = \begin{bmatrix} -\alpha e^{-\Delta_0 T} \left(\frac{\Delta_0}{\Delta_\lambda} \sinh(\Delta_\lambda T_\lambda) + \cosh(\Delta_\lambda T_\lambda) \right) & * \\ g(X) & * \end{bmatrix} \begin{bmatrix} A_0 \\ B_0 \end{bmatrix} \quad (27)$$

with α a positive prefactor that will be omitted and $g(X)$ a function that will be discussed later. We can now consider the cancellation of the left up term of the matrix. For this, we need to remember that $T_\lambda = \pi/\lambda$ so that we get

$$\Delta_\lambda T_\lambda = \pi \sqrt{\left(\frac{\epsilon}{4\lambda} \right)^2 - 1} \quad (28)$$

so that if one sets $X = \epsilon/4\lambda$, the upper left coefficient reads up to positive constants

$$f(X) = -\frac{X}{\sqrt{X^2 - 1}} \sinh\left(\pi\sqrt{X^2 - 1}\right) - \cosh\left(\pi\sqrt{X^2 - 1}\right) \quad (29)$$

This function is of prime interest for the study of phase transition. Indeed, if the systems runs for a long time at negative times, the oscillator oscillates as $\Psi(t) = A_0 e^{\Delta_0 t} e^{it} + h.c.$ as the exponentially decaying part can be neglected. Although the amplitude is not fixed, the oscillation phase is fully determined by the one of A_0 . If one now waits long enough after the defect, the same remarks holds and the oscillation phase is determined by the one of A_2 . Therefore, the sign of $f(X)$ directly encodes if there is a phase transition or not.

The latter is shown in Fig. 1a and it is positive for $X < X_c \approx 0.68$. This means that the phase transition occurs for

$$\lambda < \lambda_c = \frac{\epsilon}{4X_c} \epsilon \approx 0.37\epsilon \quad (30)$$

In other words, when the detuning is too large, no phase transition occurs while it occurs when the detuning is small. The phase diagram obtained through direct numerical simulation of the pendulum for different values of ϵ and λ is shown in 1b. The prediction is shown for comparison and excellent agreement is found even when ϵ is as big as 0.5.

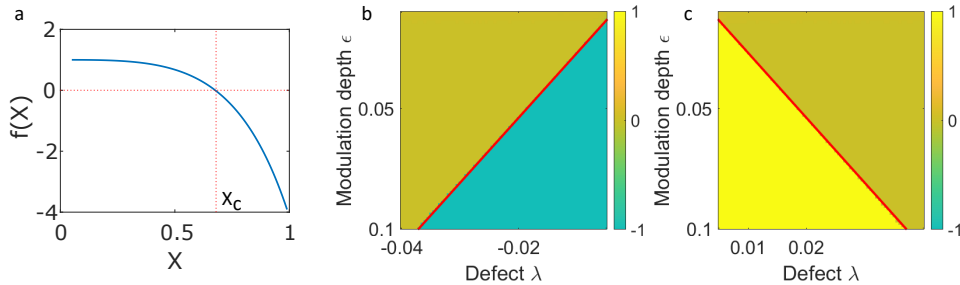


Figure 1: (a) Upper left coefficient of the transfer matrix. The sign of f changes for $X_c \approx 0.68$ indicating a phase transition. (b-c) Direct numerical simulation of the phase diagram, the colorbar encoding the value of Q . The analytical prediction for the phase transition is shown in red for comparison.

2 Analysis of the transition time T_c

We are now focusing on what happens near the transition meaning $X = X_c + \delta X$. In that case, one can approximate $f(X) \approx f'(X_c)\delta X$. On the other hand, one can show that the bottom left coefficient $g(X)$ in Eq. 27 does not cancel at X_c and takes value $g(X_c)$. We assume that before the defect, the system has run long enough so that one has $A(t < 0) = A_0 e^{\Delta_0 t}$ so that $B_0 = 0$. From Eq. (27), the solution after the defect reads

$$A(t) = A_2 e^{\Delta_0 t} + B_2 e^{-\Delta_0 t} \quad (31)$$

$$= f'(X_c) e^{\Delta_0 t} \delta X + g(X_c) e^{-\Delta_0 t} \quad (32)$$

As $\delta X \ll 1$, the dynamic of this function is first dominated by the second term that exponentially decays until both terms become of the same order. At this time, the exponential growth becomes the dominant term and $A(t)$ starts to grow again toward its new limit cycle. The time at which both terms are equal therefore gives a good hint on how the transition time T_c should scale. From the previous equation, we see that this occurs for

$$|\delta X| \sim e^{-2\Delta_0 T_c} \quad (33)$$

so that we get at the end (as $\delta X \sim \lambda - \lambda_c$)

$$T_c \sim \ln |\lambda - \lambda_c| \quad (34)$$

that is the scaling law discussed in the main text. For this argument to hold, the convergence time toward the limit cycle when the non-linearity has to be taken into account must be negligible compared to T_c . This is always the case if one takes $\lambda - \lambda_c$ small enough. In this case, the system spends 'a lot of time' near zero in the phase space so that the non-linearity can be neglected for most of the convergence process.

In our numerical simulations, this time is computed the following way. We first compute $\psi(t)$ from a standard Runge-Kutta 4 method. We then compute the associated $A(t)$ through the transformation (5). Running the simulation long enough ensures the convergence of $A(t)$ at large time toward its final value A_c . The transition time is then computed as the maximum time after the defect where $A(t)$ is still far enough from A_c . More precisely, one computes

$$T_c = \max \{t > T_\lambda / |A(t) - A_c| > \epsilon/3\} \quad (35)$$

the choice of $\epsilon/3$ being a bit arbitrary but relevant for most of the considered cases. Changing the $1/3$ factor changes the value of T_c but not the observed scaling law $T_c \sim \ln |\lambda_c - \lambda|$

3 Experimental methods and data analysis

The experimental setup consists in a tank of $5 \times 5 \text{ cm}^2$ filled with tap water as shown in Fig. 2a. The water depth is more than a couple of centimeters so that the exact value of the depth is irrelevant. The tank is placed on a shaker (B& K 4809) and vibrated with a sinus signal generated with a generator

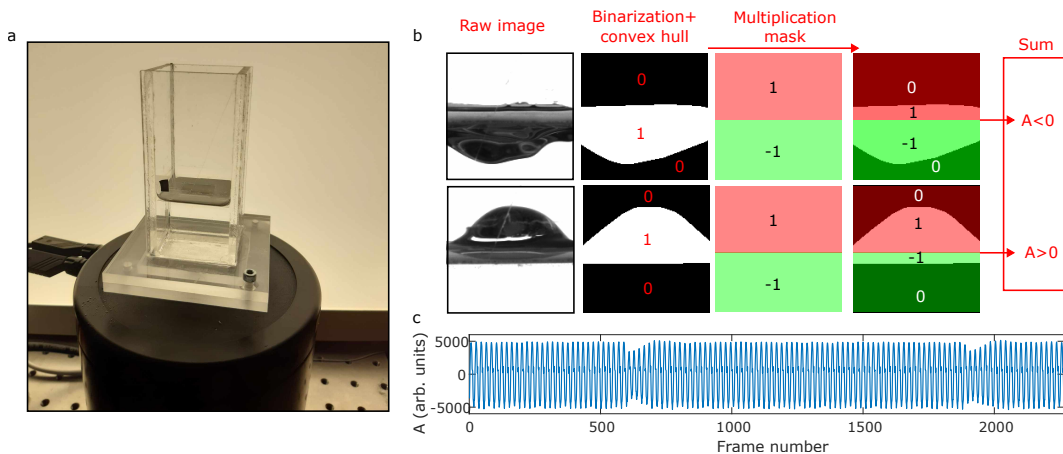


Figure 2: (a) Picture of the experimental setup: a tank filled with water is placed on a shaker. A plastic sheet is placed at the surface to prevent water waves to appear near the walls and a black mark is placed on the tank to recover its oscillatory motion. (b) Image processing method: starting from raw image of waves, we perform binarization and convex hull computation. At this stage, the number of white pixels encodes the amplitude of the wave. In order to distinguish the case of waves above and below the plastic sheet, we multiply by an analyzing mask before summing the resulting image. (c) Example of wave amplitude measurement on a movie using the previous method.

(Rigol DG1022Z) and amplified with a dedicated amplifier (B&K 2706). When the forcing amplitude is large enough, large amplitude Faraday waves oscillating at $f_0/2$ appear at the surface. In order to avoid friction on the walls, we place a transparent plastic sheet on top of the surface with a square hole of $2 \times 2 \text{ cm}^2$ on its center. The sheet prevents the instability to occur near the walls and pin the meniscus of the fluid on the edges of the square. As the sheet is floating on the water surface, evaporation does not affect the relative position of the water surface with respect to the sheet, ensuring constant boundary conditions during the whole experiment (typically several hours).

The excitation frequency f_0 is chosen so that the forcing needed to trigger the instability at $f_0/2$ is minimal, meaning that we excite the most unstable subharmonic mode. Depending on the exact experimental conditions (the room temperature appearing to be the most important), this frequency can drift a bit and typically changes between 16 Hz and 18 Hz depending on the day. For the measurement presented in the article, we have measured at the beginning of the experiment that the most unstable mode occurred for a forcing at $f_0 = 16.5 \text{ Hz}$ (modes excited with forcing at 16 Hz and 17 Hz were more stable). The resulting waves oscillate at 8.25 Hz. We used this configuration for the whole experimental measurement of the phase diagram. When the forcing is started, a growing phase of the parametric waves occurs with a typical growth time that depends on the amplitude of the forcing, but that is never larger than a few seconds. The amplitude of the waves then eventually saturates due to non-linearity and the system reaches a limit cycle.

The wave amplitude is measured by placing a camera on the side of the tank. In order to have good temporal resolution, 160 images/second are taken, what ensures approximately 10 images per oscillation of the shaker and 20 images per oscillation of the wave. A LED panel is placed behind the tank and its position is adjusted so that the background appears white while the deformed liquid interface is black as shown in Fig. 2b. A black mark (see Fig. 2) is also placed on the tank and its position is tracked along time to recover the motion of the tank due to the shaking. This measurement is used to numerically compensate the motion of the tank so that it appears as non-moving in the wave movie. The algorithm used to recover the wave amplitude is described hereafter and summarized in Fig. 2b. We first apply a binarization process followed by a convex hull computation on raw images as shown in Fig. 2b. We then multiply the resulting image by a mask that discriminates whether the wave interface is above or below the plastic sheet, and sum all the pixels of the resulting image. The result of the sum is then with good approximation the wave amplitude. As we only focus on its phase, knowing the exact prefactor to go from our measurement to an amplitude measurement in physical units is nevertheless irrelevant in our case, and we therefore plot all the results in arbitrary units. A typical measurement result is shown in Fig. 2c.

In order to introduce a temporal defect as described in the main text, we use the frequency shift keying (FSK) functionality of the function generator that allows to switch the excitation frequency between two values f_0 and f_1 depending on the value of an external 0/1 trigger signal generated by the second channel of the generator. We then chose a given value of λ , set $f_1 = f_0(1 + \lambda)$ and generate a trigger signal that is in the 1 state during $T_\lambda = 1/|f_0 - f_1|$ and that is in the 0 state for $T_d = 8$ s. The time T_d was chosen large enough so that after each defect of duration T_λ , the system could reach again a limit cycle with properly defined phase. We then record the wave amplitude for approximately 30 seconds, so that the wave experiences at least three time a temporal defect. This allows to test the reproducibility of the result for each value of λ , which were not found to vary significantly from one realization to the other. The corresponding point in the phase diagram is then found by performing standard amplitude and phase measurement on the experimental results.